Int J Adv Manuf Technol (2009) 40:67–73
DOI 10.1007/s00170-007-1322-3

ORIGINAL ARTICLE

Experiment, modeling, and analysis for temperature field of milling insert

Guangjun Liu · Guangyu Tan · Guanghui Li

Received: 25 June 2007 / Accepted: 16 November 2007 / Published online: 19 December 2007

Abstract This paper presents a theoretical and experimental study of the dynamic temperature field on a milling insert with complex groove. Experimental measurements of milling temperature using the thermocouple technique were performed. A mathematical model of the temperature field of the insert was established. A finite element model of the insert was built to simulate the temperature field. The boundary condition was determined by the experimental data and mathematical calculation, and then the temperature field of the milling insert was simulated through finite element analysis. The temperature distribution in a cut-in/cut-out cycle was obtained.

Keywords Temperature field · Milling insert · Complex groove · Finite element analysis

1 Introduction

About 90% of the energy generated in the milling process is transferred to heat, which causes a temperature increase [1]. Cutting temperature strongly influences tool life, tool fracture, and cutting force. It is well known that the cutting force and temperature are the radical reasons for tool fractures. Tool failure results directly from poor stress and temperature distributions in milling processes [1]. Currently, industries are adopting milling inserts with grooves on the rake face to improve cutting performance of the tool. It has been proven that the milling insert with three-dimensional (3D) complex groove has better cutting performance than the insert with a plane face. Tooling manufacturers now offer a great number of complex insert groove geometries [2]. The trend is to use the inserts with grooves more and more, replacing the inserts with plane faces.

In practical machining operations, grooved tools are used to effectively curl and break the chips into small sizes and shapes [3]. Complex 3D chip curl/chip form has been extensively investigated. The effect of 3D chip flow in grooved tools and the corresponding influence of the chip groove parameters on tool wear patterns were analyzed by Jawahir [3, 4]. Jawahir and Luttervelt [5] also presented a comprehensive review on the historical development of chip flow and chip curl models. It has been shown that the tool wear patterns are significantly affected by the combined effects of cutting conditions and chip groove configurations [6]. Deshayes [2] proposed a method to select the operational cutting speed range and presented a model for cutting force prediction for complex grooved tools. Jawahir and Wang [7] developed a numerical model for 2D cutting with a grooved tool insert and extended the model to include the cyclic chip formation.

As chip form and chip breakability are considered basic requirements in machining, there are many studies on chip form/chip breakability for grooved tools [8]. Many models for predicting chip curl and machining variables for machining with grooved tools have been proposed [9]. However, the design of complex grooves is rarely studied [10]. This is due to the lack of understanding of the role grooves play in machining and the difficulty to design grooves with predictable performance. A new type of milling insert with 3D complex grooves, a waved-edge insert, was developed by Li and Rong [11]. The milling

G. Liu (✉)
College of Mechanical Engineering, Tongji University,
Shanghai 200092, People's Republic of China
e-mail: lgj973@163.com

G. Tan · G. Li
Engineering College, Guangdong Ocean University,
Zhanjiang 524005, People's Republic of China

force model of the waved-edge insert was established based on the milling force model of the line-edge milling insert. It was pointed out that the temperature distribution of the grooved insert was also important but its application has not been studied widely [12–14]. Studies on temperature and stress distributions have practical meaning to optimize and develop milling inserts with the new groove.

In this paper, in order to determine the actual performance of an insert with complex grooves relative to the temperature field, experimental measurements of milling temperature were performed. The temperature field was modeled according to heat transfer theory and experimental data. Then the temperature field was analyzed by using the finite element method. Simulation of the temperature field can provide references for the evaluation of temperature distribution and can be used in the optimization of grooves.

2 Experimental methodology

Experimental measurements of milling temperature using the thermocouple technique were performed to help establish the mathematical expression of the temperature field and the boundary condition for finite element analysis.

Temperature data acquisition was performed using an improved thermocouple method [12]. The temperature measurement was achieved by a thermocouple embedded in the tool. The front end of the thermocouple was welded on the point where the temperature was to be measured. As shown in Fig. 1, the recorded signal was first amplified and transmitted through a collection ring. Then the signal was transmitted toward the acquisition device by the collection ring. An amplifier circuit was placed in the front end of the collecting ring and rotated with the spindle to reduce error. The set-up of the thermocouple is shown in Fig. 2.

A milling insert with 3D complex groove (a waved-edge insert, as shown in Fig. 3) was used in the experiment. Six points were selected to install the thermocouple. At the selected points, a hole was drilled in the bottom of the tool with an EDM machine to embed the thermocouple. The diameter of the holes was 1.5 mm and the depth of the holes was 3.2 mm. The coordinates (mm) of points 1–6 were (2.0, 2.0), (2.0, 3.5), (2.0, 5.0), (3.5, 2.0), (3.5, 3.5), and (3.5, 5.0), respectively. Six inserts were used in the experiment, and for each insert a hole was drilled according to the above-mentioned coordinates. Calibration was performed before the experiment to determine the relationship between the temperature and the output voltage.

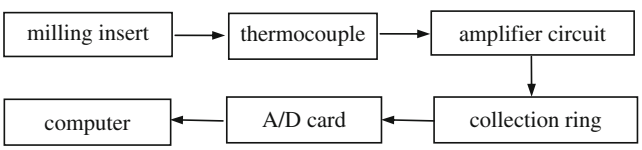

Fig. 1 Experimental system

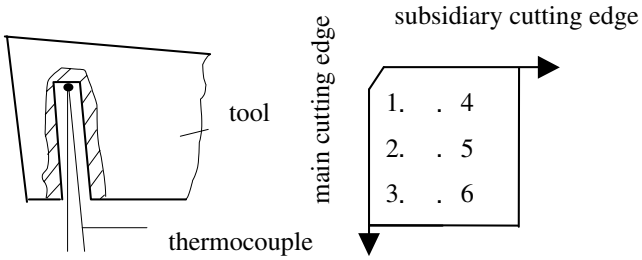

a

b

Fig. 2 Set-up of the thermocouple. **a** Schematic diagram. **b** Experimental set-up

Milling temperature measurement was performed on a vertical milling machine. The cutter head diameter was 160 mm. The workpiece material was 1045 steel. The workpiece dimensions were 83 mm in width and 200 mm in length. The FAS-4DEE-2 dynamic data acquisition system [12] was used in the experiment and with it the

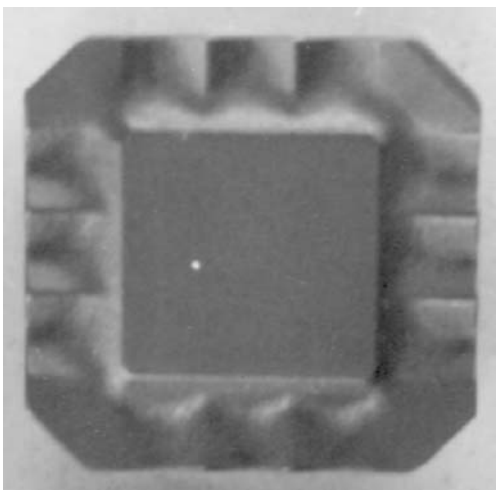

Fig. 3 Waved-edge insert used in the experiment

Table 1 Geometric parameters of the insert

Rake angle (°)	Backing-off angle (°)	Blade obliquity (°)
8	7	+15~−15

temperatures of the six points on the tools were acquired. The geometric parameters of the insert are shown in Table 1, and milling parameters are shown in Table 2. The cutting parameters used in the experiment are the combination of parameters given in Table 2. A series of experiments was conducted.

3 Modeling for the temperature field of the insert

The heat source in milling can be modeled as a finite plane heat source [15]. The solution of the finite plane heat source can be achieved from the temperature field of a point heat source. The temperature field (Fig. 4) at time t under the point heat source can be calculated according to heat transfer theory such that [15]:

$$\theta = \frac{Q_d}{c\rho(4\pi at)^{3/2}} e^{-\frac{x^2+y^2+z^2}{4at}} \tag{1}$$

where

Q_d is the heat generated at the point heat source (cal);
ρ is the density of the heat conducting medium (g/cm^3);
c is the specific heat of the heat conducting medium (cal/g·°C);
a is the coefficient of temperature conductivity of the heat conducting medium (cm^2/s);
t is the time after the heating source starts to generate heat (s); and
x, y, z are the coordinates in the heat conducting medium (cm).

According to the superposition principle of the temperature field, the calculation of temperature distribution can be derived in various conditions. Therefore, the calculation of the temperature field with finite heat source will be discussed. Figure 5 shows a finite line heat source with length L in an infinite heat conducting medium. The temperature increase at a point $M(x,y,z)$ due to the heat generated by the heat source dz_i within t seconds is:

$$d\theta = \frac{Q_s dz_i}{c\rho(4\pi at)^{3/2}} \cdot e^{-\frac{x^2+y^2+(z-z_i)^2}{4at}} \tag{2}$$

The total temperature increase resulting from the entire line heat source is:

$$\theta = \frac{Q_s}{c\rho(4\pi at)^{3/2}} \cdot e^{-\frac{x^2+y^2}{4at}} \cdot \int_0^L e^{-\frac{(z-z_i)^2}{4at}} dz_i \tag{3}$$

Let $\frac{z-z_i}{\sqrt{4at}} = u$, then Eq. 3 becomes:

$$\theta = \frac{Q_s}{2c\rho(4\pi at)} \cdot e^{-\frac{x^2+y^2}{4at}} \cdot \left[erf\left(\frac{z}{\sqrt{4at}}\right) - erf\left(\frac{z-L}{\sqrt{4at}}\right) \right] \tag{4}$$

Table 2 Cutting parameters of the experiment

Milling parameters		
Cutting parameters	Spindle speed (r/min)	220, 270, 385, 550
	Feed rate (mm/s)	19, 36, 68, 78, 84
	Depth of cut (mm)	1, 2, 3

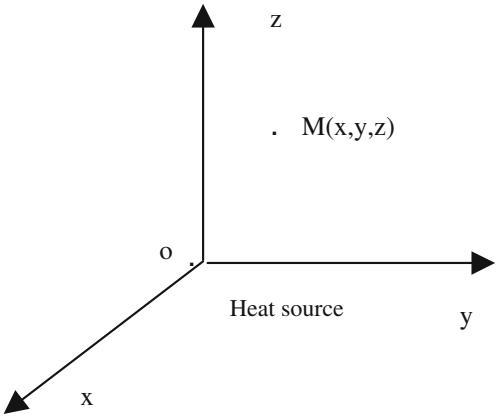

Fig. 4 Temperature field of point heat source

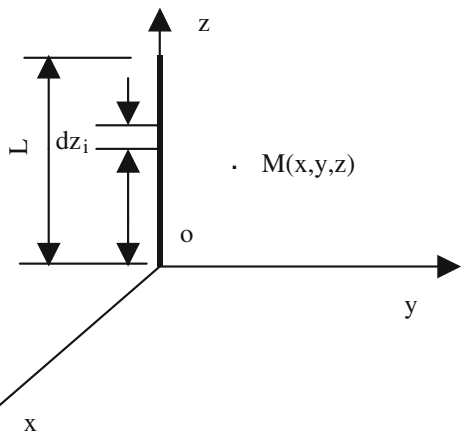

Fig. 5 Temperature field of finite line heat source

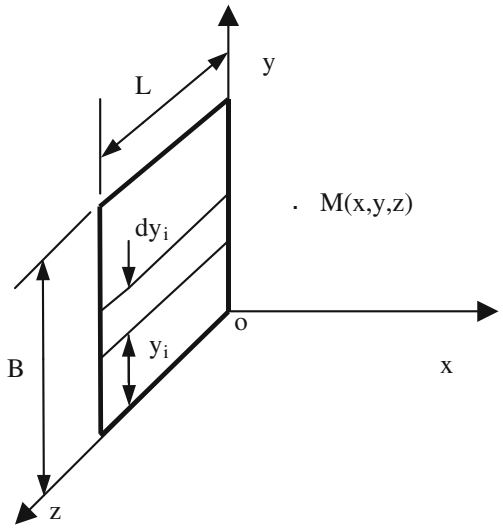

Fig. 6 Temperature field of finite plane heat source

where $erf(p) = \frac{2}{\sqrt{\pi}} \int_0^p e^{-u^2} du$ is the error function [16], which can be obtained by calculation or retrieved from a mathematical handbook. Equation 4 represents the temperature field of the finite line heat source.

The temperature field of a finite plane heat source can be derived from temperature fields of finite line heat sources [15]. As shown in Fig. 6, if there is a plane heat source with length L, width B, and the generated heat is Q_m, the temperature increase at the point $M(x,y,z)$ after t seconds can be calculated. The plane heat source can be divided into a number of narrow planes or line heat sources. According to Eq. 4, the temperature increase at point M resulting from dy_i is:

$$d\theta = \frac{Q_m dy_i}{2c\rho(4\pi at)} \cdot e^{-\frac{x^2+(y-y_i)^2}{4at}} \cdot \left[erf\left(\frac{z}{\sqrt{4at}}\right) - erf\left(\frac{z-L}{\sqrt{4at}}\right)\right] \tag{5}$$

The total temperature increase generated by the entire plane heat source is:

$$\theta = \frac{Q_m}{2c\rho(4\pi at)} \cdot \left[erf\left(\frac{z}{\sqrt{4at}}\right) - erf\left(\frac{z-L}{\sqrt{4at}}\right)\right] \cdot e^{-\frac{x^2}{4at}} \cdot \int_0^B e^{-\frac{(y-y_i)^2}{4at}} dy_i \tag{6}$$

When the integration in Eq. 6 is solved, it becomes:

$$\theta = \frac{Q_m}{4c\rho(4\pi at)^{1/2}} e^{-\frac{x^2}{4at}} \left[erf\left(\frac{z}{\sqrt{4at}}\right) - erf\left(\frac{z-L}{\sqrt{4at}}\right)\right] \left[erf\left(\frac{y}{\sqrt{4at}}\right) - erf\left(\frac{y-B}{\sqrt{4at}}\right)\right] \tag{7}$$

Equation 7 is the temperature field with a finite plane heat source.

The temperature of the points inside the tool were measured, but the heat generated at the heat source Q_m is still unknown. Q_m can be calculated through an inverse calculation according to the experimental data and Eq. 7.

For example, from the experimental results, the temperature increase of the first point after the milling process has reached its stationary state can be estimated through curve fitting as:

$$\theta_1 = 2013495862t_1^4 - 51843592t_1^3 - 259355t_1^2 + 21604t_1 + 118 \tag{8}$$

where θ_1 is the temperature increase of the first point and $t_1$is the milling time.

The temperature profiles of each point, as shown in Fig. 7, are calculated from the experimental measurements during a milling period after the milling reaches the stationary state.

According to Eq. 8, θ_1 can be determined by the experimental fitting curve and then substituted into Eq. 7 to determine Q_m. Then the temperature change of the tool can be calculated. Finally, the mathematical model can be expressed as below:

$$\theta = \frac{\theta_1 exp\left[\frac{-x^2+0.0064}{4a(t+1)}\right] \left[erf\left(\frac{z}{\sqrt{4a(t+1)}}\right) - erf\left(\frac{z-0.305}{\sqrt{4a(t+1)}}\right)\right] \left[erf\left(\frac{y}{\sqrt{4a(t+1)}}\right) - erf\left(\frac{y-0.137}{\sqrt{4a(t+1)}}\right)\right]}{\left[erf\left(\frac{0.2}{\sqrt{4a(t+1)}}\right) - erf\left(\frac{-0.105}{\sqrt{4a(t+1)}}\right)\right] \left[erf\left(\frac{0.2}{\sqrt{4a(t+1)}}\right) - erf\left(\frac{0.063}{\sqrt{4a(t+1)}}\right)\right]} \tag{9}$$

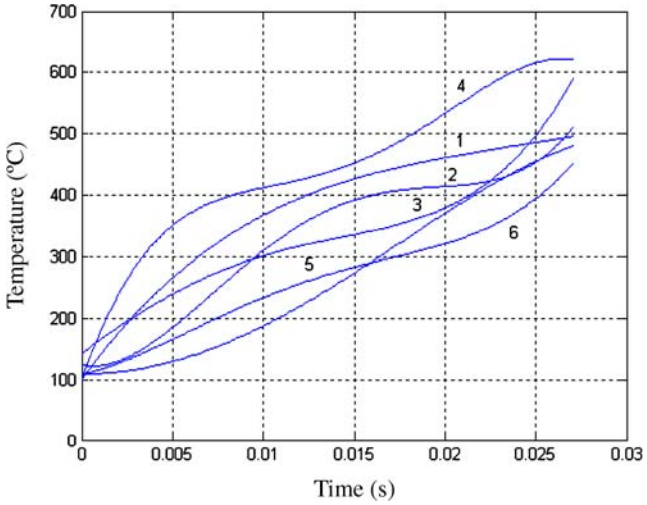

Fig. 7 Temperature–time curve of the six measuring points

4 Finite element analysis of the temperature field of the milling insert

Researchers have applied different analytical and numerical methods to investigate heat generation and cutting temperature in metal cutting [17]. Studies on the milling temperature include the calculation of cutting temperature distribution and heat flow on the tool surface [18], the mechanism of machining austempered ductile iron [19], the temperature distribution of continuous cutting and intermittent cutting where a prediction model was established [20], the temperature distribution of orthogonal cutting with a finite element analysis (FEA) heat transfer model with experiment validation of cutting force and the temperature distribution in different cutting conditions [21], the milling of austenitic steel by a finger-type cutter with FEA [22], the simulation of metal cutting by considering chip behavior and temperature distribution in the FEA model [23], the temperature distribution analysis of coated cutting tools [24], and milling of MAR-M247 nickel-based superalloy with high temperature [25]. Abukhshim and Mativenga [17] presented a comprehensive review on the heat generation and temperature prediction in metal cutting.

4.1 Modeling of the milling insert

Finite element simulations have been successfully applied for modeling cutting processes. However, the use of FEM in metal cutting research requires a large number of input parameters which need to be determined through extensive experimental work and mechanical property tests [24, 26]. The experiments and modeling of temperature fields in this work provide necessary parameters for finite element analysis.

To conduct a finite element analysis, a parametric model and meshed model of the milling insert should be established considering the characteristics of the 3D complex groove. The rake face of the waved-edge insert is a wave-curved surface, which is formed by scanning a cosine curve along a plane with an angle to the horizontal plane. The wave curve of the insert is as follows:

$$x = 0.20E - 3\cos\frac{2}{3}\pi y \tag{10}$$

where E is a parameter related to the angle between the scanning plane and the horizontal plane.

Based on Eq. 10 and the modeling method, the solid model can be built. The solid model must be meshed to generate corresponding nodes and perform the finite element analysis. Element division is a crucial step in determining the precision of the finite element analysis. Since the insert with waved-edge groove is complex in geometry, a free mesh is applied to the solid model, as shown in Fig. 8.

4.2 Finite element analysis of the temperature field

Using the meshed model and applying the temperatures acquired via experiments and calculations for the boundary conditions, a commercial tool (ANSYS) was employed to simulate the thermal process in the cutting insert during the milling operation. The results of temperature distribution are shown in Fig. 9.

From the simulation results of the finite element analysis, it can be seen that the variation of the temperature distribution changes as a function of time. It has been shown that in a milling cycle, at the beginning when the insert engages the

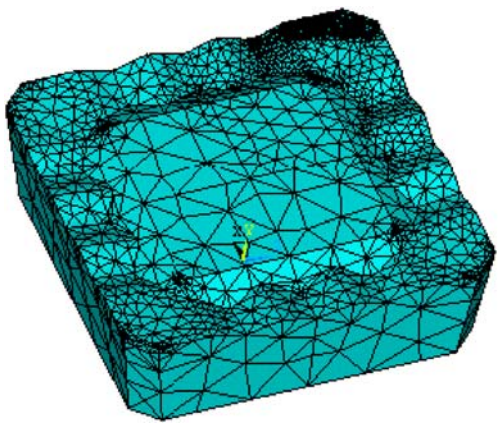

Fig. 8 Finite element model of the insert

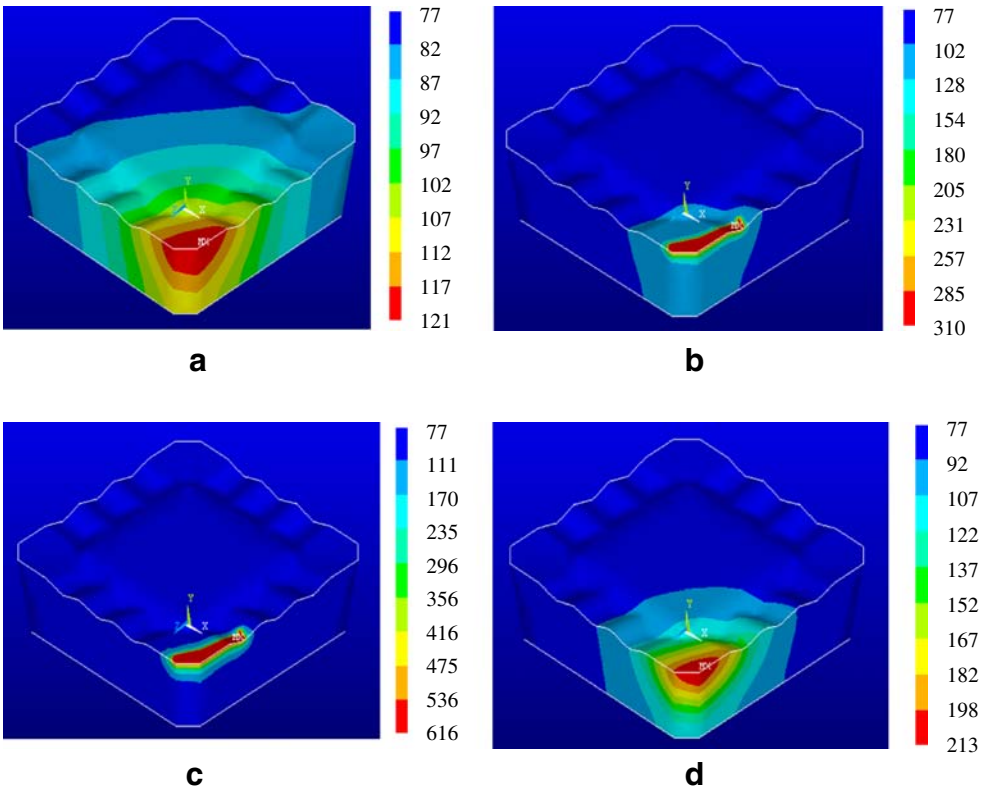

Fig. 9 Simulation results of temperature distribution. **a** Cut in. **b** 0.01 s after cut in. **c** 0.025 s after cut in. **d** Cut out

workpiece, the temperature increase is slow; however, when the insert cuts further into the workpiece, the temperature increases at a much faster rate. The maximum temperature on the rake face centralizes in the tip position of the main cutting edge. The temperature at the tool–chip interface is also high with a large temperature gradient. At cut out, the tool is cooled in air and the temperature decreases. The maximum temperature at that time is about 213°C, the maximum temperature is still in the tip position, and the tool–chip interface has a reduced temperature gradient along the rake face. Furthermore, during the cut in process, the maximum temperature climbs to more than 600°C quickly. In the milling process, the temperature gradient is very large during both the cut in and cut out processes.

The finite element analysis results may provide a better understanding and comparative evaluations for optimizing the geometric parameters of grooves, without intensive and expensive experimental tests. Based on the experiments and finite element analysis of the temperature profile and distribution of the milling insert with complex groove, this work can be continued to optimize the tool design under different conditions.

5 Conclusions

We have studied the temperature field of a milling insert with complex groove. A method for the temperature measurement of the insert is described. An amplifier circuit was placed in the front end of the collection ring and rotated with the spindle to reduce error. A dynamic data acquisition system was employed to acquire the temperature data in the milling process for further calculation and analysis.

Based on heat transfer theory, the mathematical expression of the temperature field has been established to determine the boundary conditions for the finite element analysis. The finite element analysis study on the 3D temperature field of the milling insert with complex groove was conducted in a cut in and cut out cycle. The distribution and change rule of the temperature field was obtained.

The simulation method can provide a reference for insert groove design, tool wear monitoring during machining, choice of optimal cutting parameters for given tools and materials, and the influence of coatings without intensive experiments.

Acknowledgments The authors would like to acknowledge the support of the National Science Foundation of China (50575062), the Specialized Research Fund for the Doctoral Program of Higher Education (20060214002), and the Key Project for Abroad Scholar of Education Department of Heilongjiang Province (1151HZ003).

References

1. Tan G, Yuan J, Wang X, Yuan ZJ (1997) Cause for exit failure of end mill. J Harbin Inst Technol 4(7):107–111
2. Deshayes L (2007) Analysis of an equivalent tool face for the cutting speed range prediction of complex grooved tools. J Mater Process Technol 190(1–3):251–262
3. Ee KC, Balaji AK, Jawahir IS (2003) Progressive tool-wear mechanisms and their effects on chip-curl/chip-form in machining with grooved tools: an extended application of the equivalent toolface (ET) model. Wear 255(7–12):1404–1413
4. Jawahir IS, Li PX, Ghosh R, Exner EL (1995) A new parametric approach for the assessment of comprehensive tool-wear in coated grooved tools. CIRP Ann 45(1):49–54
5. Jawahir IS, van Luttervelt CA (1993) Recent developments in chip control research and applications. CIRP Ann 42(2):659–693
6. Jawahir IS, Ghosh R, Balaji AK, Li PX (2000) Predictability of tool failure modes in turning with complex grooved tools using the equivalent toolface (ET) model. Wear 244(1):94–103
7. Jawahir IS, Wang X (2007) Development of hybrid predictive models and optimization techniques for machining operations. J Mater Process Technol 185(1–3):46–59
8. Ghosh R, Redetzky M, Balaji AK, Jawahir IS (1996) The equivalent toolface (ET) approach for modeling chip curl in machining with grooved tools. Proceedings of the 13th symposium on engineering applications in mechanics, McMaster University, ON, Canada, pp 702–711
9. Zhang H, Dillon OW, Jawahir IS (2001) A finite element analysis of 2D machining with a grooved tool. Transactions of the North American Manufacturing Research Institution of SME (XXIX):327–334
10. Li G, Liu G, Tan G, Li Z, Rong Y (2005) Reconstruction technique of 3D complex groove of milling insert based on genetic algorithms. Chinese J Mech Eng 41(6):113–117
11. Li Z, Zhang Z, Yan F, Dong L, Tao H, Wei Y, Rong Y (2000) Waved-edge insert development and milling force model. Chinese J Mech Eng 36(10):42–45
12. Tan G, Liu G, Li Z, Liu M, Li G, Rong Y (2004) 3D temperature field analysis and fuzzy comprehensive evaluation for milling insert with complex groove. Chinese J Mech Eng 40(3):106–110
13. El Hossainy TM, El-Shazly MH, Abd-Rabou M (2001) Finite element simulation of metal cutting considering chip behavior and temperature distribution. Mater Manuf Process 16(6):803–814
14. Elmoussami H, Battaglia JL (2003) A method to estimate the average temperature on the cutting edge of tools: application on the milling process. Exp Heat Transf 16(2):139–158
15. Hou ZB, He SJ, Li SX (1984) Heat conduction in solids. Shanghai Science and Technology Press, China
16. Poppe GPM, Wijers CMJ (1990) More efficient computation of the complex error function. ACM Trans Math Softw 16(1):38–46
17. Berliner EM, Knainov VP (1991) Analytic calculation of the temperature field and heat flows on the tool surface in metal cutting due to sliding friction. Wear 143(2):379–395
18. Masuda M, Sato T, Kori T, Chujo Y (1994) Cutting performance and mechanism of alumina-based ceramic tools when machining austempered ductile iron. Wear 174(1–2):147–153
19. Radules R, Kapoor SG (1994) An analytical model for prediction of tool temperature fields during continuous and interrupted cutting. J Eng Ind 116(22):135–143
20. Liu D, Yu X, Lou P (1999) Finite element analysis of the temperature distribution in orthogonal metal machining. J Beijing Inst Technol 8(4):386–391
21. Fel'adshtein EE, Kaminski VL (2001) Modeling of the thermal field of a workpiece in milling of austenitic steel by a finger-type cutter. J Eng Phys Thermophys 74(1):149–152
22. El Hossainy TM, El-Shazly MH (2001) Finite element simulation of metal cutting considering chip behavior and temperature distribution. Mater Manuf Process 16(6):803–814
23. Du F, Lovell MR (2001) Boundary element method analysis of temperature fields in coated cutting tools. Int J Solids Struct 38 (26–27):4557–4570
24. Abukhshim NA, Mativenga PT, Sheikh MA (2006) Heat generation and temperature prediction in metal cutting: a review and implications for high speed machining. Int J Mach Tools Manuf 46(7–8):782–800
25. Hsu CY, Huang CK, Wu CY (2007) Milling of MAR-M247 nickel-based superalloy with high temperature and ultrasonic aiding. Int J Adv Manuf Technol 34(9–10):857–866
26. Astakhov VP (2007) Effects of the cutting feed, depth of cut, and workpiece (bore) diameter on the tool wear rate. Int J Adv Manuf Technol 34(7–8):631–640